

Calendar effect on phase study in paleoclimate transient simulation with orbital forcing

Guang-Shan Chen · J. E. Kutzbach ·
R. Gallimore · Zhengyu Liu

Received: 29 March 2010 / Accepted: 2 November 2010 / Published online: 17 November 2010
© Springer-Verlag 2010

Abstract Several studies have shown that the use of different calendars in paleoclimate simulations can cause artificial phase shifts on insolation forcing and climatic responses. However, these important calendar corrections are still often neglected. In this paper, the phase shifts at the precession band is quantitatively assessed by converting the model data of the transient GCM climate simulation of Kutzbach et al. (Clim Dyn 30:567–579, 2008) from the “fixed-day” calendar to the “fixed-angular” calendar with a new and efficient approach. We find that insolation has a big phase shift in September–October–November (SON) when the vernal equinox (VE) is fixed to March 21. At high latitude, the phase bias is up to 60° (about 3650 years). The insolation phase bias in SON in Southern Hemisphere (SH) is especially important because it can influence the timing of the SH summer monsoon response due to the large heat capacity of ocean. The calendar correction has minor effect ($\pm 2^\circ$) on the phase relationships between forcing and precipitation responses of the six global summer monsoons studied in Kutzbach et al. (2008). After correcting the calendar effect, especial on SH ocean temperature, the new phase wheel results are more similar for both hemispheres. The results suggest that the calendar effect should be corrected before discussing the dynamics between orbital forcing and climatic responses in phase studies of transient simulations.

Keywords Calendar effect · Phase study ·
Orbital forcing · Transient simulation

1 Introduction

Following pioneering work of Milankovitch (1941), various geological records from ocean, loess deposits, ice cores and cave speleothems clearly demonstrate that the variations of Earth’s orbital parameters are the main driving forcing for climate change on orbital time scales. To investigate the response of the climate to orbital perturbations, Global Climate Models (GCMs) have been extensively used. During the past three decades, the response of the climate has been studied by using the time slice approach to evaluate the quasi-equilibrium climate responses to prescribed orbital and lower boundary conditions, such as ice volume, and greenhouse gasses (Kutzbach 1981; Kutzbach and Otto-Bliesner 1982; Hewitt and Mitchell 1998; Montoya et al. 2000; Liu et al. 2003)—so-called “snapshot simulations”. Very recently, advances in computer speed and acceleration techniques have made it possible to simulate the continuous evolution of long-term climate in response to time-dependent orbital forcing (Jackson and Broccoli 2003; Lorenz and Lohmann 2004; Liu et al. 2006; Timmermann et al. 2007; Kutzbach et al. 2008)—so-called “transient simulations”. With transient paleoclimate simulations, we are now able to study the phase relation between forcing and climate responses in the climate system on orbital time scales (Kutzbach et al. 2008; Chen et al. 2010) in the same way as with geological records (Clemens et al. 1991).

To analyze the model output, one needs to define a calendar to calculate and save monthly averages (most common). There are two ways to define a calendar. The

G.-S. Chen (✉)
SKLLQG, Institute of Earth Environment,
Chinese Academy of Sciences, Xi’an, China
e-mail: gchen9@gmail.com

G.-S. Chen · J. E. Kutzbach · R. Gallimore · Z. Liu
Center for Climate Research, University of Wisconsin,
Madison, WI, USA

first way defines months following the present-day calendar for any period of the past with the vernal equinox (VE) fixed at March 21 noon or with the autumnal equinox (AE) fixed at September 23 noon. Here we refer to this calendar as a “fixed-day” calendar, which is equivalent (in name) to the “classical” calendar defined by Joussaume and Brannonot (1997, henceforth JB) and the “fixed” calendar defined by Timm et al. (2008). Typically, a fixed-day calendar is defined with VE fixed at March 21 (hereinafter the VE is fixed at March 21 noon for the fixed-day calendar unless we mention). For simplicity, some models also use 360 days in one year and 30 days per month.

The second way uses a “fixed-angular” calendar (the name adopted by Timm et al. (2008)). This approach has been used in only a few GCM simulations (for example, Kutzbach and Gallimore 1988; Mitchell et al. 1988; JB 1997). The “fixed-angular” calendar is defined as follows: Each month begins and ends at the same celestial longitude as present-day for any period, with the VE designated as 0° celestial longitude. In the “fixed-angular” calendar, insolation is in phase for any period of the past and the response of climate keeps the same phase relationship relative to insolation and solar geometry.

The two calendars are equivalent for present, but are different in the length of the seasons when the orbital parameters change (JB 1997; Kutzbach and Gallimore 1988; Thomson 1995). Following Kepler’s second law (the time elapsed between two positions of the Earth along the ellipse is proportional to the area covered), the angular velocity of the Earth is not constant through a year due to the elliptical shape of the Earth’s orbit and, most importantly here, this angular velocity changes due to the phase of the precession. Therefore the number of days between the equinoxes or in a given month is not fixed. In JB, they showed the length of each month of the fixed-angular calendar at 126 ka BP (a time when Earth is at perihelion during North Hemisphere (NH) summer and orbital eccentricity is large (~ 0.04) compared to present (~ 0.015)) (Table 1). With NH summer perihelion and large eccentricity, the length of NH summer (JJA) at 126 ka BP is 9 days shorter for the fixed-angular calendar. In addition, January 1st for the fixed-angular calendar at 126 ka BP is on day 354 of the fixed-day calendar.

Two important studies have shown the effect of the two calendars on amplitude and phase shift of insolation forcing and climatic responses in paleoclimate simulations (JB 1997; Timm et al. 2008). As shown in Fig. 3b in JB, if one compares the insolation difference between 126 ka BP and present using the “fixed-day” calendar (Fig. 1b), the patterns of differences exhibit a north-south tilt structure as a function of season, with insolation about 50 W/m^2 lower at NH high latitudes in September and about 60 W/m^2 higher at SH high latitudes in October. This tilt structure would be

Table 1 Starting day, ending day, and length of month for 126 ka BP on the fixed-day calendar and the fixed-angular calendar for a 360-day year

	Fixed-day			Fixed-angular		
	Starting	Ending	Length	Starting	Ending	Length
Jan	1	30	30	354	26	33
Feb	31	60	30	27	59	33
Mar	61	90	30	60	90	31
Apr	91	120	30	91	120	30
May	121	150	30	121	148	28
Jun	151	180	30	149	175	27
Jul	181	210	30	176	202	27
Aug	211	240	30	203	229	27
Sep	241	270	30	230	258	29
Oct	271	300	30	259	288	30
Nov	301	330	30	289	320	32
Dec	331	360	30	321	353	33

The starting day and ending day are referred to the first day of the year in the fixed-day calendar

changed to a south-north orientation in spring with the AE fixed at September 23 (Fig. 3d in JB). Using the “angular” calendar to compare the insolation difference between 126 ka BP and present, the tilt structure totally disappears (Fig. 1c). The insolation differences show a symmetric structure. This pattern is independent on any time reference. We note that making corrections for this tilt structure (Fig. 1b) is still not given enough attention in paleoclimate simulations, despite the repeated explanations (Timm et al. 2008)—possibly due in part to the additional post-processing required.

We show the calendar bias (the values on the fixed-day calendar minus the values on the fixed-angular calendar) on insolation at 126 ka BP in Fig. 1d. The insolation is about 50 W/m^2 lower at NH high latitudes during July–August–September–October for the fixed-day calendar than that for the fixed-angular calendar. At SH high latitudes, the insolation is about 50 W/m^2 higher during SON for the fixed-day calendar than for the fixed-angular calendar. Even in the middle latitudes, the differences are still about $\pm 30 \text{ W/m}^2$.

Corresponding to the calendar bias on insolation in Fig. 1d, calendar biases are also found for SON Surface temperature (Fig. 2a) and precipitation (Fig. 2b). The calendar bias for SON surface temperature (Fig. 2a) is between 4 and 5°C (cooler) over the Eurasian continent and the Northern American continent and about 2°C (warmer) over Antarctica. The calendar bias for SON precipitation is largest in tropical and middle latitudes (Fig. 2b), about ± 2 to ± 4 . JB noted that these calendar biases on climatic responses are statistically significant.

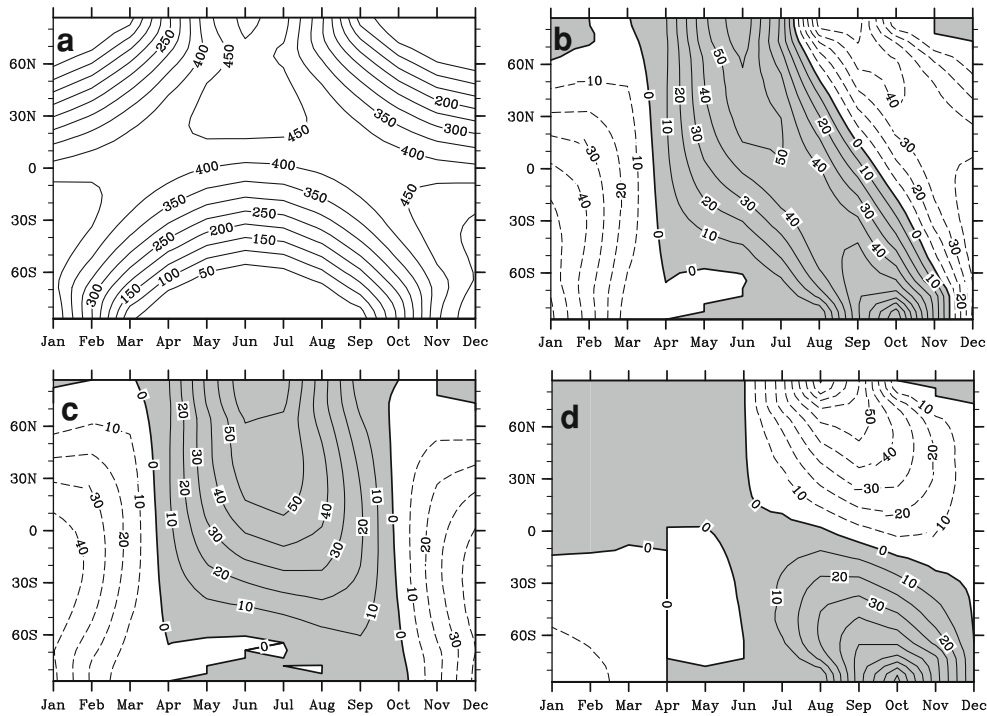
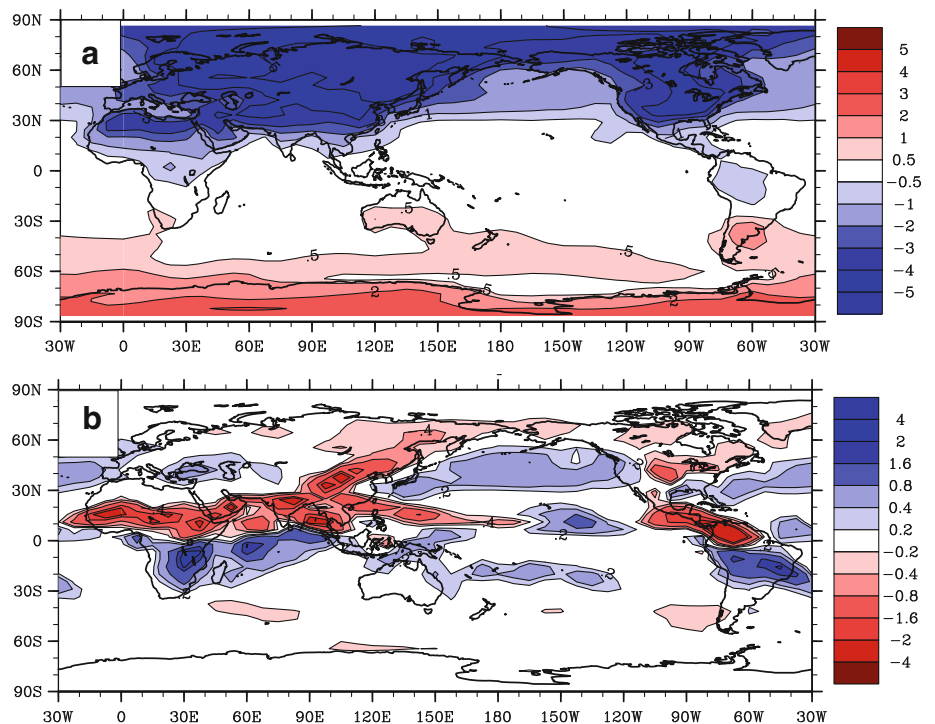


Fig. 1 Monthly mean insolation (W/m^2) at the top of the atmosphere as a function of latitude for **a** present, **b** 126 ka BP on the fixed-day calendar minus present, **c** 126 ka BP on the fixed-angular minus present, **d** calendar bias for 126 ka BP (values on the fixed-day

calendar minus values on the fixed-angular calendar at 126 ka BP). The vertical zero line in April in (**d**) is the result of the contouring algorithm

Fig. 2 Calendar bias on: **a** SON surface temperature ($^{\circ}C$), **b** SON precipitation (mm/day) at 126 ka BP. Calendar bias is the difference between the values on the fixed-day calendar and the values on the fixed-angular calendar at 126 ka BP (fixed-day calendar minus fixed-angular calendar)



Timm et al. (2008) found artificial phase shifts of climate response due to the calendar effect in transient simulations by visual examination of the time series of

Indian monsoon rain in autumn for the two calendars (Fig. 8 in Timm et al. 2008). They mentioned the importance of using the fixed-angular calendar in process studies

(transient simulations) and noted the particular concern about monsoons, with emphasis on the Indian monsoon. It is worthily to point out that the GCMs simulations themselves (with timestep) are not affected by the choice of calendar. The above calendar biases and artificial phase shifts occurs only when the model data are post-processed as monthly means or seasonal means.

Transient paleoclimate simulations are more and more used to study the dynamics of the climate system on orbital time scales (Kutzbach et al. 2008; Chen et al. 2010). In Kutzbach et al. (2008) (hereafter KLLC), we proposed that insolation-forced controls on precipitation for the six monsoon regions are thermal dynamic (land/ocean temperature contrast) and hydrologic dynamic (evaporation from the ocean, and landward transport of water vapor related to SST). However, in KLLC, we used the fixed-day calendar and did not consider the calendar effect on phase shifts between forcing and response. Given the large phase shifts in autumn illustrated in Timm et al. (2008) and our own earlier concerns about calendar corrections, we now re-examine the results presented in KLLC.

In this paper, we use a new calendar conversion method to convert the model data of KLLC from the fixed-day calendar to the fixed-angular calendar to quantitatively assess the calendar effect on phase in an insolation-forcing-only transient simulation by cross-spectral analysis. We describe the data used and our conversion method in Sect. 2. The effects of our correction are discussed in Sect. 3. In Sect. 4, we apply our method to the transient simulation in KLLC and present the new (corrected) phase results. Conclusion and discussion are in Sect. 5.

2 Data and method

2.1 Data

We use three datasets in our study. The first dataset is the model data of the accelerated transient simulation over the last 284,000 Kyr published in KLLC and Chen et al. (2010). The transient simulation was performed using FOAM (version 1.5) with an acceleration scheme. In the transient simulation, the insolation forcing was accelerated by 100 times (the orbital forcing was updated by 100 years for each year of model simulation). Other boundary conditions, such as the continental ice sheets, sea level and greenhouse gasses, were kept the same as present day. The descriptions of the FOAM model, the acceleration scheme, the experiment design and the cross-spectral analysis technique are in KLLC and Chen et al. (2010). The model data were saved as monthly averages using the fixed-day calendar.

The second dataset is a snapshot run data at 126 ka BP produced by FOAM (version 1.5). The surface boundary conditions of the snapshot run are identical to present-day. Atmospheric CO₂ concentration is prescribed at the pre-industrial level (280 ppmv). The model was spun up for 150 years and then daily data were saved for the next 50 years. The daily data were post-processed to monthly averages based on the fixed-day calendar and the fixed-angular calendar, respectively. Climatological averages over the last 50 years are used.

The third dataset is daily insolation data calculated following the approach of Berger (1978). This dataset has the same time coverage as the accelerated transient simulation (over the last 284,000 years). Then the daily insolation data were post-processed to monthly mean insolation data based on the two calendars.

The first dataset is used to assess the calendar effect on phase analysis in the transient run. The second and the third dataset are used to verify our method.

2.2 Method

To obtain monthly means directly on the fixed-angular calendar, one needs to save model output as daily data, and then post-process the daily data as monthly averages according to the definition of the fixed-angular calendar. This is impracticable due to computer time and storage capacity limitations for a long transient simulation. However, an approximate estimation of monthly means on the fixed-angular calendar is feasible by converting the data from the fixed-day calendar to the fixed-angular calendar via post-processing. Two methods have been described recently: one by Pollard and Reusch (2002) (hereafter PR), the other by Timm et al. (2008).

There are two steps in the PR method. Step one: interpolate the monthly mean values for a particular variable and grid point on the fixed-day calendar to daily mean values. Step two: average the daily data to monthly data for the fixed-angular calendar. In the first step, the PR conversion method uses a parabola ($a + b.t + c.t^2$ where t is time) as a continuous function to generate daily data from the given 12 monthly means, requiring the same monthly means as the originals, and continuity of value and slope at the month boundaries. This results in 36 linear equations for 36 unknowns (12 months \times 3 parabolic coefficients), which can be solved by Gaussian elimination. Then the daily data are averaged to new monthly means according to the definition of the fixed-angular calendar. The PR method can significantly reduce the calendar effect for most variables, but fails for precipitation in the ITCZ region (see PR). They also tried to use a cubic ($a + b.t + c.t^2 + d.t^3$) as a continuous function to generate daily data and noted

that the two continuous functions gave virtually identical results.

The method used in Timm et al. (2008) decomposed the differences ($d(\tau)$) between the fixed-day calendar and the fixed-angular calendar into

$$d(\tau) = d_0(\tau) + \tilde{d}(\tau)$$

in which

$$d_0(\tau) = [A_c - A_a(\tau)]X_0$$

$$\tilde{d}(\tau) = [A_c - A_a(\tau)]\tilde{X}(\tau)$$

where τ is the orbital year; $d_0(\tau)$ is the effect of the fixed-day calendar versus the fixed-angular calendar on the preindustrial annual cycle; $\tilde{d}(\tau)$ is the effect of the fixed-day calendar versus the fixed-angular calendar on the change in the annual mean cycle; X_0 is the preindustrial annual cycle; $\tilde{X}(\tau)$ is the orbital driven change in the annual mean cycle; A_c is the fixed-day calendar, $A_a(\tau)$ is the fixed-angular calendar at the orbital τ year. They used daily data of the mean preindustrial annual cycle (X_0) to estimate $d_0(\tau)$ and neglected $\tilde{d}(\tau)$. This correction significantly reduced the calendar bias in their Earth system model of intermediate complexity (EMIC). But they noted that their method might have limitations in correcting for larger changes in climatic variables in GCMs with a full and large seasonal cycle. They suggested that their method should be compared with the PR method when applied to GCMs results.

Our method for converting model data from the fixed-day calendar to the fixed-angular calendar is similar to the PR method. However, to generate the daily data in step one we only use linear interpolation for the portions of the two calendar months that don't overlap and we use the same values as the monthly mean for the portions of the two calendar months that overlap. The explanations are given below.

The monthly averages on the fixed-day calendar and on the fixed-angular calendar for an arbitrary field T are,

$$T_D = 1/D_D \sum T \tag{1}$$

$$T_A = 1/D_A \sum T \tag{2}$$

where T_D and T_A are the monthly averages on the fixed-day calendar (D indicates Day) and on the fixed-angular calendar (A indicates Angular), respectively. D_D and D_A are, respectively, the number of days comprising each average.

T_D and T_A can be divided into two parts: the part that is overlapped and the part that is separated in the two averages. Equations 1 and 2 are thus modified to

$$T_D = 1/D_D \sum T_O + 1/D_D \sum T_{\bar{O}D} \tag{3}$$

$$T_A = 1/D_A \sum T_O + 1/D_A \sum T_{\bar{O}A} \tag{4}$$

where T_O refers to the part of the field T which is contained in both averages; $T_{\bar{O}D}$ ($T_{\bar{O}A}$) refers to the non-overlapped part in the field T_D (T_A). For example, the fixed-angular January for 126 ka BP has days 1–26 in common with the fixed-day January (Table 1). The sum of the field T in days 1–26 is $\sum T_O$. The fixed-day January has days 27–30 that are not a part of the fixed-angular January. The sum of the field T in days 27–30 is $\sum T_{\bar{O}D}$. The fixed-angular January has days 354–360 that are not a part of the fixed-day January. The sum of the field T in days 354–360 is $\sum T_{\bar{O}A}$ (see Table 1).

We use Eq. 3 to express $\sum T_O$ in term of the known calendar monthly average T_{D1} ,

$$\sum T_O = D_D T_D - \sum T_{\bar{O}D} \tag{5}$$

Substituting Eq. 5 into (4) we have

$$T_A = \frac{D_D}{D_A} T_D - \frac{1}{D_A} \sum T_{\bar{O}D} + \frac{1}{D_A} \sum T_{\bar{O}A} \tag{6}$$

In Eq. 6, D_D , D_A , and T_D are known. To calculate T_A , we need to estimate $\sum T_{\bar{O}D}$ and $\sum T_{\bar{O}A}$. The daily values of $T_{\bar{O}D}$ and $T_{\bar{O}A}$ are estimated by linear interpolation of the monthly means T_D assigned to the fixed-day calendar mid-month. As an example, let us consider the process of estimating the January average on the fixed-angular calendar for 126 ka BP (T_{A1}). The values of D_D and D_A in Eq. 6 are 30 and 33 days. The monthly averages on the fixed-day calendar for December, January and February (T_{D12} , T_{D1} and T_{D2}) are known. $\sum T_{\bar{O}A}$ is determined from the interpolated daily estimates using T_{D12} assigned to day 345 and T_{D1} assigned to day 15. $\sum T_{\bar{O}D}$ is determined from the interpolated daily estimates using T_{D1} assigned to day 15 and T_{D2} assigned to day 45.

3 Validation of the method

We verify our method by checking the correction on amplitude of insolation forcing, surface temperature and precipitation responses using the second datasets and by checking the correction on phase of insolation forcing using the third datasets. Also we compare the converted results of our method with that of the PR method. Note that we only compare our method with the PR method (recalling Timm's et al. (2008) suggestion regarding use of correction techniques with GCMs data).

3.1 Amplitude correction

Converting the insolation data on the fixed-day calendar in the second dataset with the two methods, we obtain the estimated insolation data on the fixed-angular calendar. Residual biases (the estimated values minus the true values

on the fixed-angular calendar) are used to show the accuracy of the conversion method. Between 60°N and 60°S, the residual bias of our method on insolation (Fig. 3a) is less than 2 W/m². It can, however, reach 4–12 W/m² at very high latitudes (75°N/S to the pole). The residual bias of the PR method (Fig. 3b) on insolation is less than 2 W/m² over most latitudes. At high latitudes it can reach 4 W/m². Compared to the calendar bias in Fig. 1d, the residual bias (Fig. 3a, b) is very small everywhere.

After correction for the calendar effect, the residual bias for SON surface temperature is below 0.4°C with our method (Fig. 3c) or below 0.2°C with the PR method (Fig. 3d). The residual bias for SON precipitation is about 0.2 mm/day or less (Fig. 3e, f) for both methods. Compared to the calendar bias in Fig. 2, the calendar-related bias on temperature and precipitation are very significantly reduced. PR had noted a more substantial residual bias on precipitation in the tropics based on only a 10-year average

from a 25-year run. But by using the 50-year average from the 200-year 126 ka BP experiment, we find the residual bias on precipitation in the tropics is very small for both methods.

3.2 Phase correction

Computer time limitation prevented us from re-running our transient simulation (KLLG) over last 284,000 years and saving daily data to calculate the exact monthly data averaged on the fixed-angular calendar. But there is one way to calculate the exact monthly insolation data averaged on the fixed-angular calendar and on the fixed-day calendar by post-processing the daily insolation data following the approach of Berger (1978) over last 284,000 years. With the two conversion methods, estimated monthly insolation data on the fixed-angular calendar are calculated. Using these three insolation data sets (monthly mean insolation

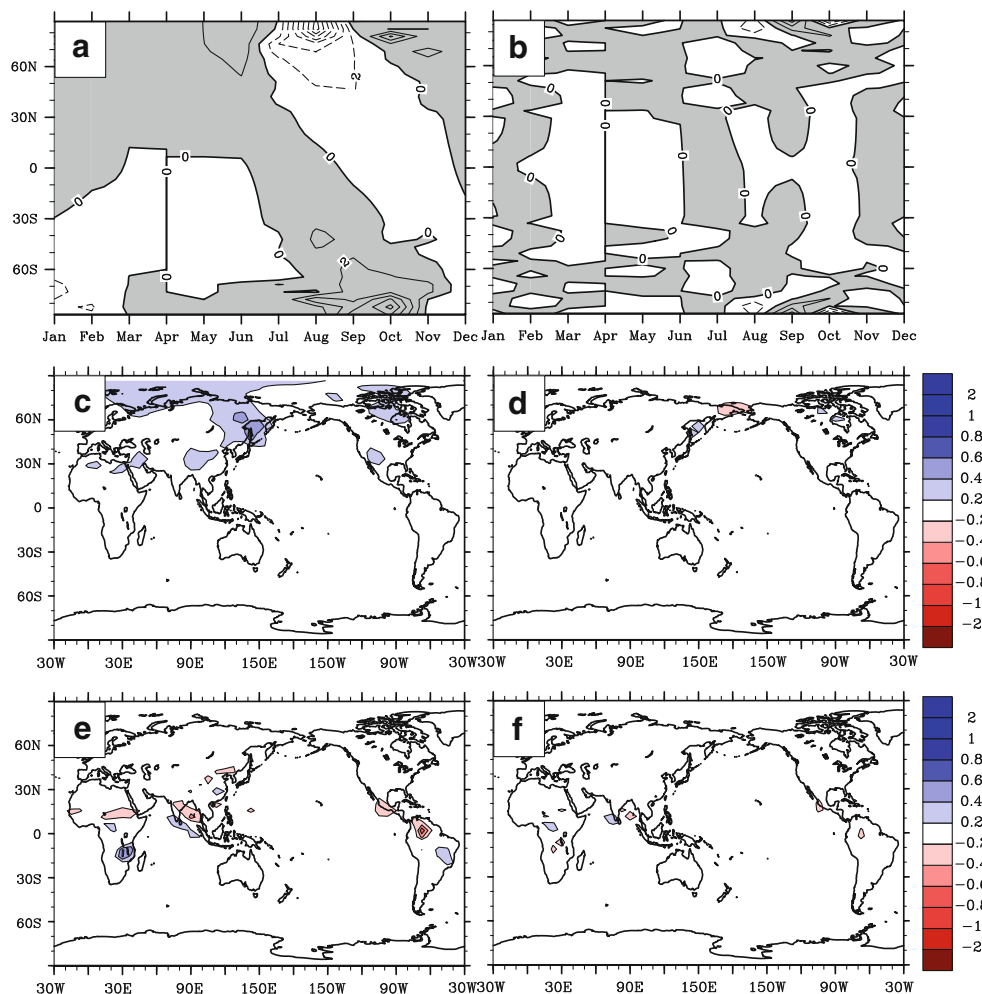


Fig. 3 Residual bias on insolation (W/m²) (a, b), SON surface temperature (°C) (c, d), SON precipitation (mm/day) (e, f) at 126 ka BP using our method (a, c, e) and the PR method (b, d, f). Residual bias is the difference between the estimated values on the fixed-

angular calendar and the true values on the fixed-angular calendar at 126 ka BP (estimated values minus true values on the fixed-angular at 126 ka BP)

Table 2 Calendar bias and residual bias on phase ($^{\circ}$) for insolation forcing at the precession band obtained from cross-spectrum analysis of the insolation data over last 284,000 years

	11 $^{\circ}$ N		33 $^{\circ}$ N		60 $^{\circ}$ N	
	Calendar bias	Residual bias	Calendar bias	Residual bias	Calendar bias	Residual bias
Jan	3	-2 (-2)	15	-1 (-2)	107	-2 (-2)
Feb	1	-2 (-2)	5	-2 (-2)	51	-1 (-1)
Mar	0	-2 (-2)	-1	-2 (-2)	-2	-2 (-2)
Apr	0	-2 (-2)	1	-2 (-2)	2	-2 (-2)
May	-1	-2 (-2)	2	-2 (-2)	6	-2 (-2)
Jun	-2	-2 (-2)	-1	-2 (-2)	0	-2 (-2)
Jul	-2	-1 (-2)	-12	-2 (-2)	-34	-4 (-2)
Aug	-7	-1 (-2)	-30	-2 (-2)	-64	-5 (-2)
Sep	-17	-2 (-1)	-42	-3 (-2)	-68	-6 (-2)
Oct	-20	-3 (-1)	-40	-4 (-1)	-62	-4 (-2)
Nov	-15	-3 (-1)	-28	-3 (-2)	-49	3 (-1)
Dec	-3	-1 (-1)	-5	-1 (-1)	-13	2 (-1)

A positive (negative) phase means the monthly insolation data averaged using the fixed-day calendar or the estimated monthly insolation data averaged using the fixed-angular calendar leads (lags) the true monthly insolation data averaged using the fixed-angular calendar. The residual biases are from our method; the values in the parentheses are from the PR method. Coherence at the precession band exceeds 0.97 in all cases

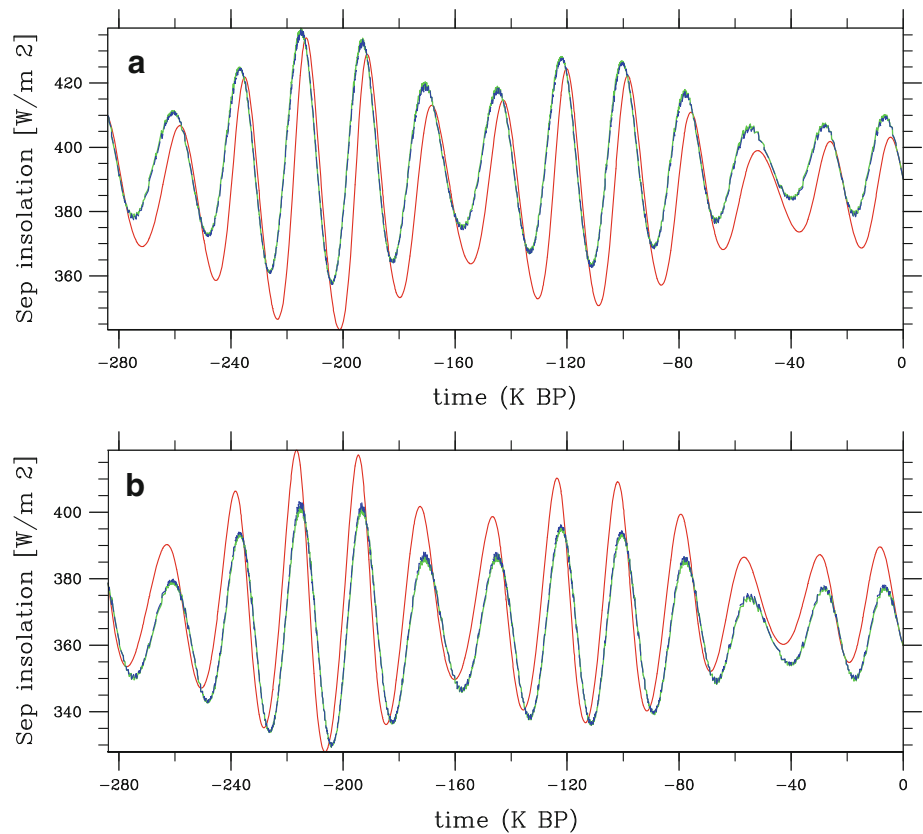
on the fixed-day calendar, monthly mean insolation on the fixed-angular calendar, estimated monthly mean insolation on the fixed-angular calendar), we can assess the calendar effect on insolation phase and thereby validate our conversion method for phase bias. The calendar biases and residual biases on insolation phase at the precession band for each month are shown in Table 2. The phase values in Table 2 are calculated by cross-spectrum analysis (Jenkins and Watts 1968; Imbrie et al. 1989) on the two insolation time series over the span of 284,000 years. For example, the calendar bias on phase of January insolation at 11 $^{\circ}$ N (3 $^{\circ}$ in Table 2) is calculated by a cross-spectrum analysis between the January insolation time series averaged on the fixed-day calendar and the true January insolation time series averaged on the fixed-angular calendar. The residual bias on phase is calculated in the same way, except using the estimated time series averaged on the fixed-angular calendar to replace the time series averaged on the fixed-day calendar.

We find that the calendar biases on insolation phase are small ($\pm 2^{\circ}$) at all latitudes (low latitudes 11 $^{\circ}$ N, middle latitudes 33 $^{\circ}$ N, high latitude 60 $^{\circ}$ N) in March, April, May, and June at the precession band (Table 2). We note that all the calendar biases on phase are calculated based on the VE is fixed to March 21 in the fixed-day calendar. But the calendar biases on phase are large at all latitudes in September, October, and November (SON). At high latitude, it is up to 60 $^{\circ}$ (about 3650 years, a precession period of 22,000 years is used to convert degree to years). Phases in years are rounded the nearest 50 years. For example, the calendar bias for June insolation at middle latitude is -1 $^{\circ}$,

i.e., the June insolation on the fixed-day calendar lags the June insolation on the fixed-angular insolation by 1 $^{\circ}$. However, the calendar bias for September insolation at middle latitude (33 $^{\circ}$ N) is -42 $^{\circ}$, i.e., the September insolation on the fixed-day calendar lags the September insolation on the fixed-angular calendar by 42 $^{\circ}$. This large phase lag can be seen by visual examination of the time series of the September insolation for the two calendars in Fig. 4a. Figure 4b shows the time series of the September insolation for the two calendars at SH middle latitude (33 $^{\circ}$ S). One can see that the September insolation on the fixed-day calendar leads the September insolation on the fixed-angular calendar at SH middle latitude. As expected, the SH lead/lag relationship for September insolation is opposite to the phase relationship of the NH September insolation owing to the different (and opposite) effects that JJA perihelion has the September insulations in the two hemispheres (Fig. 1b). We note that the phase biases due to the calendar effect in SON are comparable with or even larger than the physical phase lag between 2 adjacent months (about 30 $^{\circ}$). The reason for the calendar bias being small in MAM and large in SON is that the VE is fixed at March 21 noon. With the VE fixed at March 21, the insolation in MAM is kept almost in phase. But the insolation in SON (6 months after the reference day) has a large phase shift. We note that calendar biases would be large in MAM and small in SON if the AE is fixed at September 23.

After correction, the residual bias on phase of September insolation at the precession band is -3 $^{\circ}$ (-2 $^{\circ}$) with our method (the PR method), which also can be seen in Fig. 4a

Fig. 4 Time series of September insolation for: **a** NH middle latitude, **b** SH middle latitude. *Red solid line* is the time series on the fixed-day calendar. *Green solid line* is the time series on the fixed-angular calendar. *Blue dashed line* is the estimated time series on the fixed-angular calendar



(dashed blue line and solid green line). Generally, the residual biases in Table 2 are less than 5° for our method and are less than 2° for the PR method. These residual biases are quite small compared to the fixed-day calendar biases themselves.

Figure 3 and Table 2 show that the calendar effect both on amplitude and phase can be significantly reduced with the two correction methods. We note our method works well, though the residual biases on amplitude and phase of the PR method are somewhat smaller compared with those of our method. However, our method has the advantage of being 13 times faster (computer time) than the PR method. This factor of 13 is perhaps not important for short transient experiments but it becomes very important when converting multiple-thousand-year transient simulations data due to the limitation of computer resources. It results not only in computer savings but savings in time required by the scientist to post-processes results efficiently.

4 Calendar effect on phase study in KLLC

KLLC discussed the phase response of global summer monsoons to precession forcing over the past 284,000 years using the fixed-day calendar (no post-processing correction).

Here, we use our method and the PR method to convert the model output of KLLC from the fixed-day calendar to the fixed-angular calendar and then redo the phase analysis of KLLC to evaluate the calendar bias on phase responses in the transient run. The regions referred to in Tables 3 and 4 are shown in Fig. 5.

The calendar biases on phase response of summer surface temperature for the NH mid-latitude land (NLD) and oceans (NPC, NAT, NTO) are quite small (about $\pm 2^\circ$) (Table 3, which corresponds to Table 1 in KLLC). The same is true for the summer surface temperature of the SH mid-latitude land (SLD). However the calendar biases of summer surface temperature over the SH mid-latitude oceans (SPC and SAT) are large (about 15° – 20°). There is a phase lead (a positive phase bias) between the surface temperature on the fixed-day calendar and the surface temperature on the fixed-angular calendar over SH mid-latitude ocean. Before calendar correction, the phases of surface temperature over NPC, NAT, and NTO are almost same (around 40°), whereas the phases of surface temperature over SPC, SAT, and STO are different. The phase of surface temperature over SPC or SAT is about 15° larger than that of surface temperature over STO. After correction, the surface temperature over the tropical ocean has the same phase as the surface temperature over the mid-latitude ocean in both hemispheres.

Table 3 Phases of the summer surface temperature averaged on both calendars for NH (SH) mid-latitude lands and oceans with respect to minus precession index at the precession band obtained from cross-spectrum analyses of the transient run

Region	Fixed-day phase (°)	Fixed-angular phase (°)	Phase bias (°)
NH			
NLD	4	2 (2)	2 (2)
NPC	36	39 (40)	-3 (-4)
NAT	31	32 (33)	-1 (-2)
NTO	39	42 (42)	-3 (-3)
NLD-NTO	-11	-8 (-8)	-3 (-3)
SH			
SLD	4	1 (1)	3 (3)
SPC	45	29 (28)	16 (17)
SAT	45	28 (27)	17 (18)
STO	32	28 (29)	4 (4)
SLD-STO	-26	-22 (-22)	-4 (-4)

A positive (negative) phase means the surface temperature leads (lags) the minus precession index. Phase bias = phase on the fixed-day calendar - phase on the fixed-angular calendar. The phases in the parentheses are calculated from the data estimated by the PR method. Coherence at the precession band exceeds 0.97 in all cases. *Note:* In KLLC, all phases are calculated relative to NH Jun insolation for NH climate variables and SH December insolation for SH climate variables. The precession index (eccentricity times the sine of the angle between the perihelion and the moving vernal equinox) is multiplied by -1, so that the NH Jun (SH December) insolation has $\sim 0^\circ$ phase with minus precession index. The locations of the regions are shown in Fig. 5

Table 4 Phases of the summer precipitation averaged on both calendars for the six monsoon regions with respect to the minus precession index at the precession band obtained from cross-spectrum analyses of the transient run

Region	Fixed-day phase (°)	Fixed-angular phase (°)	Phase bias (°)
NH			
NAF	-1	-5 (-5)	4 (4)
SAS	23	21 (21)	2 (2)
NAM	14	13 (13)	1 (1)
SH			
SAF	3	2 (4)	1 (-1)
NAU	-19	-17 (-19)	-2 (-2)
SAM	-15	-15 (-15)	0 (0)

A positive (negative) phase means the precipitation leads (lags) the minus precession index. Phase bias = phase on the fixed-day calendar - phase on the fixed-angular calendar. The phases in the parentheses are calculated from the data estimated by the PR method. Coherence at the precession band exceeds 0.97 in all cases. *Note:* In KLLC, all phases are calculated relative to NH Jun insolation for NH climate variables and SH December insolation for SH climate variables. The NH Jun (SH December) insolation has $\sim 0^\circ$ phase with the minus precession index (see the definition of the minus precession index in the caption of Table 3). The locations of the regions are shown in Fig. 5

Why are the calendar biases over the NH ocean and over the SH ocean different in summer? In KLLC, we found that the sea surface temperature (SST) of a given month has maximum coherence and $\sim 0^\circ$ phase with the insolation forcing of 2 months earlier due to the large heat capacity of the ocean, exhibiting a phase lag between forcing and response over ocean. In other words, NH (SH) summer SST over ocean has $\sim 0^\circ$ phase with May (October) insolation. From Table 2, we can see that the calendar bias on phase of May insolation at mid-latitude is small. Therefore the calendar bias is small for the summer SST of the NH mid-latitude. Figure 4b shows the September insolation at SH mid-latitude has a large phase bias (35°) between the two calendars, which explains the large phase bias on the summer surface temperature over SH mid-latitude ocean. The months in this example are rounded for illustrative purposes. Also the phase lead between the insolation on the fixed-day calendar and the insolation on the fixed-angular calendar in Fig. 4b explains the phase lead between the surface temperature on the fixed-day calendar and the surface temperature on the fixed-angular calendar over the SH mid-latitude ocean (Table 3), which indicates that the insolation phase bias in SON in SH is especially important because it can influence the timing of the SH summer monsoon response due to the large heat capacity of ocean. We note that the calendar would not be an issue to analyze the phase on a long time scale in some regions, where there is no seasonal phase shift or similar phase shift in the response of ocean and land to the insolation forcing.

The calendar biases on the phase of the precipitation response for the six global summer monsoons are small (about 2°) (Table 4). It is noteworthy that calendar bias differences on phase responses of summer temperature and precipitation between our method and the PR method are very small, which indicates that our method works equally well as the PR method.

In Fig. 6, we use the corrected phases in Tables 3 and 4 to plot the corrected phase wheel to compare with the previous (uncorrected) phase results in KLLC (dashed lines and white arrows). The new phase wheel is quite similar to the previous one of KLLC in most but not all respects. All the phases of the summer precipitation for the six monsoons (3 in the NH, 3 in the SH) lie within the limits of the hydrologic process index “h” (tropical SST: NTO or STO, respectively) and the thermal process index “t” (land/ocean surface temperature difference: NLD-NTO, or SLD-STO, respectively). The only difference is that the limit of hydrological/thermal process indices becomes narrower for the SH (from $26 + 32 = 58^\circ$ to $22 + 28 = 50^\circ$) because of the correction to the SH ocean phase response (and hence more similar to the limits for the NH). Therefore the conclusion of KLLC that the controls on precipitation for

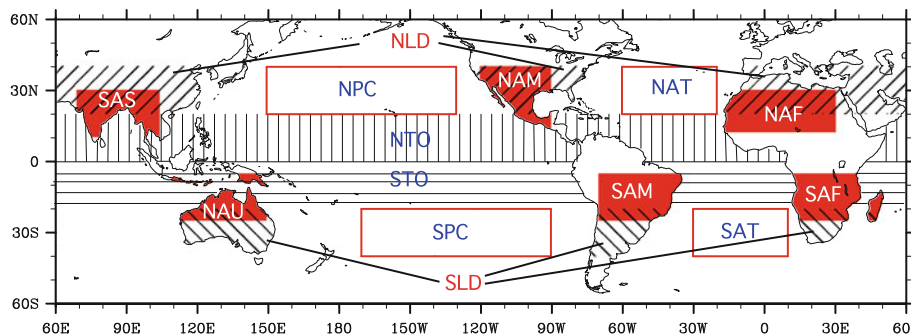


Fig. 5 Locations of area average domains for six monsoon regions and several land and ocean regions used in Kutzbach et al. (2008). The six monsoon regions include South Asia (SAS), north Australia (NAU), North American (NAM), South American (SAM), North Africa (NAF), South Africa (SAF)—shaded with red color; the four mid-latitude ocean regions include the North Pacific Ocean (NPC), North Atlantic Ocean (NAT), South Pacific Ocean (SPC), North Atlantic Ocean (NAT), South Atlantic Ocean (SAT)—red boxes. The broad regions represent climates of northern (southern) land, NLD (SLD)—slanted lines between 20 and 40°N/S, and northern (southern) tropical ocean SSTs, NTO (STO)—vertical (horizontal) lines between 0 and 20°N/S

South Pacific Ocean (SPC), North Atlantic Ocean (NAT), South Atlantic Ocean (SAT)—red boxes. The broad regions represent climates of northern (southern) land, NLD (SLD)—slanted lines between 20 and 40°N/S, and northern (southern) tropical ocean SSTs, NTO (STO)—vertical (horizontal) lines between 0 and 20°N/S

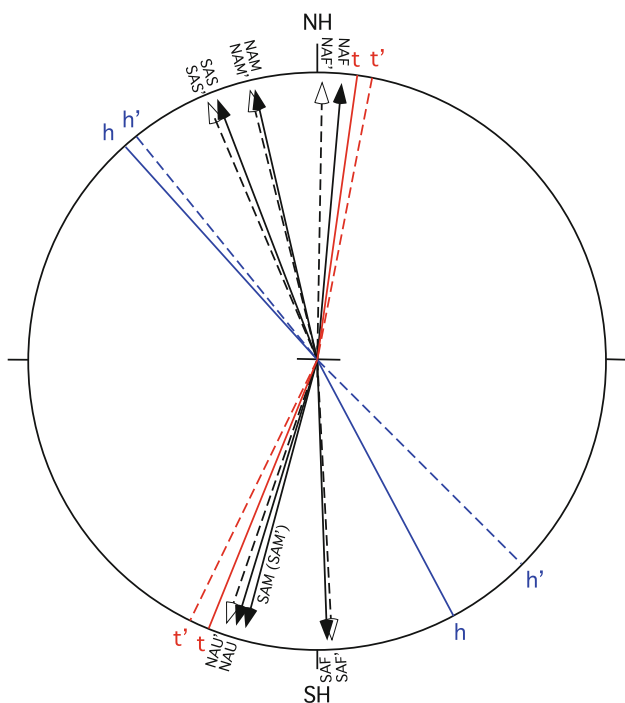


Fig. 6 Phase wheel for JJA (DJF) precipitation rate of the three northern (southern) monsoon regions, NAF, SAS, NAM (SAF, NAU, SAM), relative to northern (southern) hemisphere June (December) reference insolation, NH (SH), with phase leads (lags) shown counterclockwise (clockwise). Dashed lines with white arrow indicate the phase results in Kutzbach et al. (2008). The lines labeled with “h” (“t”) indicate the phase of hydrologic process (the process of thermal process). To illustrate the phase shift of SH ocean temperature, “h” indicates the phase of ocean temperature. The monsoon regions are labeled and described in Fig. 5

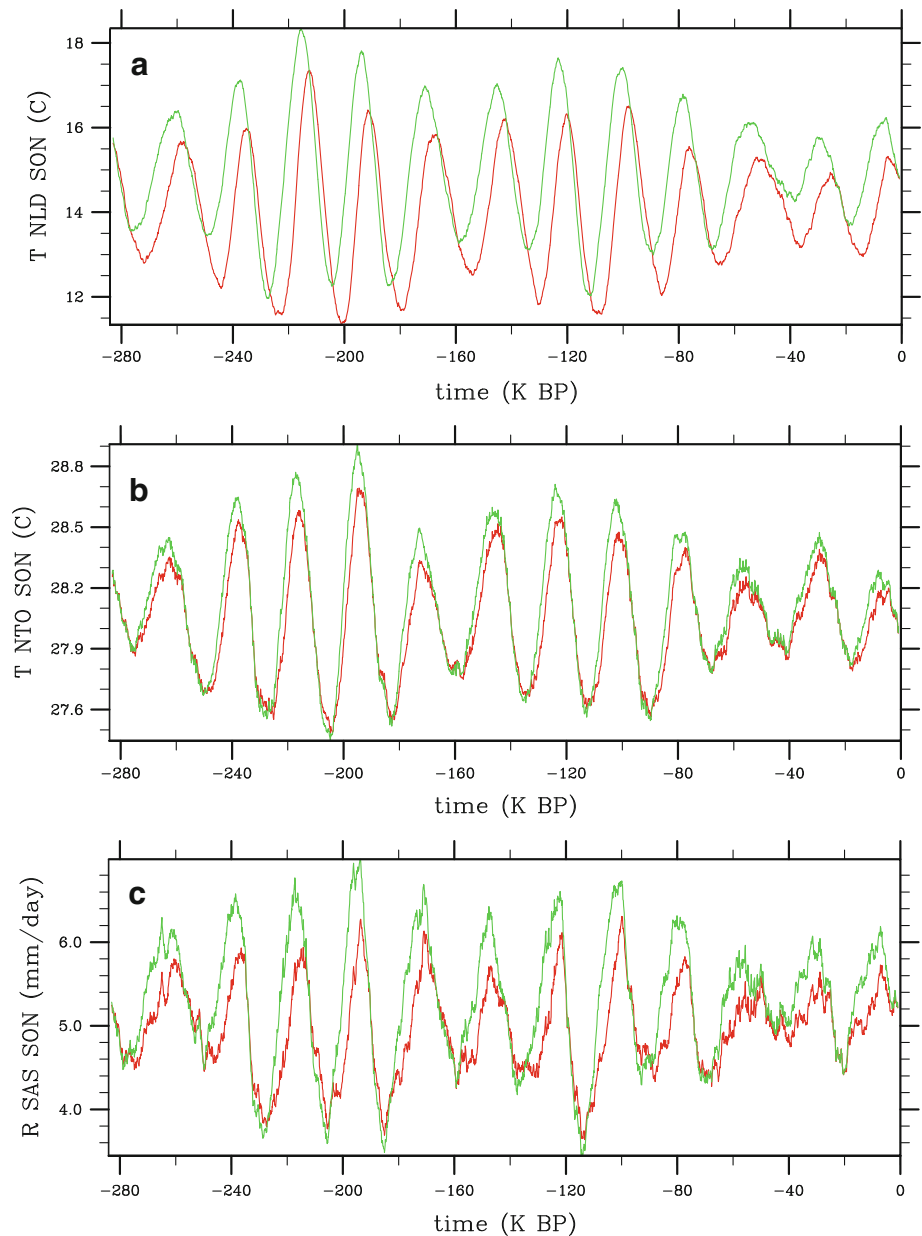
the six monsoon regions are thermal dynamic and hydrologic dynamic and their phases fall with the limit of these indices is now strengthened because these limits are now similar in both hemispheres after correction to the fixed-angular calendar.

For comparing with the results in Timm et al. (2008), time series of the northern land surface temperature (NLD), northern ocean surface temperature (NTO), and the precipitation over Indian monsoon region in SON are shown in Fig. 7. Though the calendar effect causes small phase shifts in temperature and precipitation during summer time, it causes a large phase shift on temperature and precipitation in SON (Fig. 7). The land temperature of NLD (Fig. 7a), the ocean temperature of NTO (Fig. 7b) and the precipitation over Indian monsoon region (Fig. 7c) on the fixed-day calendar (red solid line) lag those on the fixed-angular calendar (green solid line), respectively. We note that the results we find in Fig. 7a, c are the same as the results found by Timm et al. (2008). The calendar biases on the SON land surface temperature, the ocean temperature, and the precipitation over the Indian monsoon region calculated by the cross-spectral analysis are 51°, 13°, and 28°, respectively. The phase lag of the precipitation over Indian monsoon region on the fixed-day calendar can be explained by the phase lags of land surface temperature and ocean surface temperature on the fixed-day calendar.

5 Summary

The calendar biases on insolation phase between the fixed-day calendar and the fixed-angular calendar at the precession band are largest in SON season (6 months away from the anchor point). At high latitude, this bias is up to 60° (about 3650 years). The insolation phase bias in SON in SH is very important because the large heat capacity of ocean can influence the timing of the SH summer monsoon response. We expect the similar result in MAM in NH when the AE is fixed at September 23 in a fixed-day calendar. In KLLC, the calendar effect has minor bias ($\pm 2^\circ$) on the phase relationship between precession forcing and

Fig. 7 Time series of **a** northern land surface temperature, **b** northern ocean surface temperature, and **c** precipitation over SAS in SON. *Red solid line* indicates the time series on the fixed-day calendar. *Green solid line* indicates the time series on the fixed-angular calendar



the responses of temperature and precipitation for the six global summer monsoons in JJA (or DJF). But the calendar effect on the phase response of the summer ocean surface temperature in the SH is relatively large (about 15° – 20°) due to the insolation phase bias in SON. In general, the results of KLLC are more consistent for the two hemispheres when the appropriate fixed-angular calendar is applied. The conversion method described in this paper can be used to estimate the “fixed-angular” calendar monthly data from the “fixed-day” calendar monthly data. Compared with the PR method, the method in this paper works well and is more efficient (13 times faster).

Timm et al. (2008) discussed the implications of the calendar effect biases for model-data comparison. They

argued that it is important to understand the seasonal response characteristics of proxies. For the proxies with strong seasonal response functions that could be influenced by comparison with model output in fixed-day calendar format, the fixed-angular calendar correction should be applied to model output before comparison with proxy data. We strongly agree with this point. However, the main purpose of this paper was to quantitatively assess the phase shift of insolation forcing and climate variables due to the calendar definition in a transient simulation and to point out the importance of getting the model physical response correct first. Moreover, because we used only insolation forcing in the accelerated simulation in KLLC and did not include CO_2 forcing or other glacial boundary condition

forcings, we did not compare our results with paleoproxies data.

The calendar effect is particularly important for analyses of monthly or seasonal changes. For other subjects, it could be ignored. However, for most paleoclimate simulations, monthly data are saved. We join Timm et al. (2008) in recommending using the fixed-angular calendar in transient paleoclimate model simulations or one of the two methods described here to post-process transient simulation model monthly data before one explores the dynamics between forcing and climatic response or compares model output with proxy data.

Acknowledgments The authors are grateful to the editor and the two anonymous reviewers. Their constructive comments significantly improved the paper. We also thank David Pollard for providing their code. The simulations were made at the NSF-sponsored computing facility of NCAR, Boulder, Co. This work was jointly supported by US NSF grants, Natural Science Foundation of China (40825008) and National Basic Research Program of China (2010CB833406).

References

- Berger AL (1978) Long-term variations in daily insolation and Quaternary climate changes. *J Atmos Sci* 35:2362–2367
- Chen G-S, Liu Z, Clemens SC, Prell WL, Liu X (2010) Modeling the time-dependent response of the Asian Summer Monsoon to obliquity forcing in a coupled GCM: a PHASEMAP sensitivity experiment. *Clim Dyn*. doi:[10.1007/s00382-010-0740-3](https://doi.org/10.1007/s00382-010-0740-3)
- Clemens SC, Prell WL, Murray D, Shimmield G, Weedon G (1991) Forcing mechanisms of the Indian Ocean monsoon. *Nature* 353:720–725
- Hewitt CD, Mitchell JFB (1998) A fully coupled general circulation model simulation of the climate of the mid-Holocene. *GRL* 25:361–364
- Imbrie J, McIntyre A, Mix A (1989) Oceanic response to orbital forcing in the late Quaternary: observational and experimental strategies. In: Berger A, Schneider S, Duplessy JC (eds) *Climate and geosciences*. Kluwer, Boston
- Jackson CS, Broccoli AJ (2003) Orbital forcing of Arctic climate: mechanisms of climate response and implications for continental glaciation. *Clim Dyn* 21:539–557
- Jenkins GM, Watts DG (1968) *Spectral analysis and its applications*. Holden Day, Oakland
- Joussaume S, Braconnot P (1997) Sensitivity of paleoclimate simulation results to season definition. *J Geophys Res* 102(D2): 1943–1956
- Kutzbach JE (1981) Monsoon climate of the early Holocene: climate experiment with the earth's orbital parameters for 9000 years ago. *Science* 214:59–61
- Kutzbach JE, Gallimore RG (1988) Sensitivity of a coupled atmosphere/mixed-layer ocean model to changes in orbital forcing at 9000 yr BP. *J Geophys Res* 93:803–821
- Kutzbach JE, Otto-Bliesner BL (1982) The sensitivity of the African-Asian monsoonal climate to orbital parameter changes for 9000 yr B.P. in a low-resolution general circulation model. *J Atmos Sci* 39(6):1177–1188
- Kutzbach JE, Liu X, Liu Z, Chen G-S (2008) Simulation of the evolutionary response of global summer monsoon to orbital forcing over the past 280,000 years. *Clim Dyn* 30:567–579
- Liu Z, Otto-Bliesner BL, Kutzbach JE, Li L, Shields C (2003) Coupled climate simulation of the evolution of global monsoon in the Holocene. *J Clim* 16:2472–2490
- Liu Z, Wang Y, Gallimore R, Notaro M, Prentice IC (2006) On the cause of abrupt vegetation collapse in North Africa during the Holocene: climate variability vs. vegetation feedback. *Geophys Res Lett* 33:L22709. doi:[10.1029/2006GL028062](https://doi.org/10.1029/2006GL028062)
- Lorenz SJ, Lohmann G (2004) Accelerated technique for Milankovitch type forcing in a coupled atmosphere-ocean circulation model: method and application for the Holocene. *Clim Dyn* 23:727–743
- Milankovitch M (1941) *Kanon der Erdbestrahlung und seine Anwendung auf das Eiszeitenproblem*. Ed. Spec. Sect. Sci. Math. Nat. 33, Acad. Serbe, R., Belgrade
- Mitchell JFB, Grahame NS, Needham KJ (1988) Climate simulations for 9000 years before present: seasonal variations and effects of the Laurentide ice sheet. *J Geophys Res* 93(D7):8283–8303
- Montoya M, Von Storch H, Crowley TJ (2000) Climate simulation for 125,000 years ago with a coupled ocean-atmosphere general circulation model. *J Clim* 13:1057–1072
- Pollard D, Reusch DB (2002) A calendar conversion method for monthly mean paleoclimate model output with orbital forcing. *J Geophys Res* 107(D22):4615. doi:[10.1029/2002JD002126](https://doi.org/10.1029/2002JD002126)
- Thomson DJ (1995) The seasons, global temperature, and precession. *Science* 268(5207):59–68. doi:[10.1126/science.268.5207.59](https://doi.org/10.1126/science.268.5207.59)
- Timm O, Timmermann A, Abe-Ouchi A, Saito F, Segawa T (2008) On the definition of seasons in paleoclimate simulations with orbital forcing. *Paleoceanography* 23:PA2221. doi:[10.1029/2007PA001461](https://doi.org/10.1029/2007PA001461)
- Timmermann A, Lorenz S, An S-I, Clemens A, Xie S-P (2007) The effect of orbital forcing on the mean climate and variability of the tropical Pacific. *J Clim* 20:4147–4159